International Journal of Biological Macromolecules 49 (2011) 317–322

Contents lists available at ScienceDirect

International Journal of Biological Macromolecules

journal homepage: www.elsevier.com/locate/ijbiomac

Secondary structure of chorion proteins of the Lepidoptera *Pericallia ricini* and *Ariadne merione* by ATR FT-IR and micro-Raman spectroscopy

A.K. Srivastava[a,1], V.A. Iconomidou[b,1], G.D. Chryssikos[c], V. Gionis[c], K. Kumar[a], S.J. Hamodrakas[b,*]

[a] Department of Zoology, Insect Endocrinology Laboratory, University of Allahabad, Allahabad (UP) 211002, India
[b] Department of Cell Biology & Biophysics, Faculty of Biology, University of Athens, Panepistimiopolis, Athens 157 01, Greece
[c] Theoretical and Physical Chemistry Institute, National Hellenic Research Foundation, Athens 116 35, Greece

ARTICLE INFO

Article history:
Received 20 February 2011
Received in revised form 9 May 2011
Accepted 11 May 2011
Available online 19 May 2011

Keywords:
ATR FT-IR spectroscopy
Micro-Raman spectroscopy
Scanning and transmission electron microscopy
Lepidoptera eggshell (chorion) proteins
Secondary structure
Helicoidal architecture
β-Pleated sheet
Natural protective amyloids

ABSTRACT

The gross morphological features of the eggs and eggshells (chorions) of two Lepidoptera species, *Pericallia ricini* and *Ariadne merione* were revealed for the first time by scanning and transmission electron microscopy. These two insect pests are extremely serious threats for many crops, mainly in India, but also in several other regions of the world. Micro-Raman and ATR FT-IR spectroscopy were also applied to study in detail the secondary structure of the eggshell (chorion) proteins of these Lepidoptera species. Both techniques indicate that the two species have nearly identical conformations of their chorion proteins with abundant antiparallel β-pleated sheet. These results are in support of our previous findings that the helicoidal architecture of the proteinaceous chorion of Lepidoptera and fishes is dictated by a common molecular denominator, the antiparallel β-pleated sheet secondary structure.

1. Introduction

Pericallia ricini (Arctiidae), a.k.a. Castor wooly bear, is a polyphagous pest with a wide range of hosts in India and many parts of the world. Its eggs are laid in clusters on the leaves of various plants (Castor, Sunflower, Sesame, Brinjal, Pumpkin, Banana, Sweet potato, Radish, etc.) and its larvae feed on them causing complete defoliation [1]. *Ariadne merione* (Nymphalidae), a.k.a. Common Castor butterfly, is an orange butterfly flying among the foliage of Castor plants (*Ricinus communis*) and its larvae feed almost exclusively on their leaves [2]. Both, *P. ricini* and *A. merione* have proved to be extremely serious threats for many crops in many regions of the world, including India [1,2].

Besides the economic impact of these insect species, there are several other reasons for the systematic structural study of their eggs and eggshells: the morphological study could provide new and useful information for taxonomic and phylogenetic purposes, as well as about their physiology and/or demography. Also, useful clues for insect pest control could be anticipated if detailed studies at the eggshell (chorion) protein secondary structure level are provided [3].

In this work, the overall morphology of laid eggs and eggshells from both species was studied by scanning and transmission electron microscopy. In addition, detailed ATR FT-IR and micro-Raman structural studies of the eggshell (chorion) proteins were performed, to provide information about the secondary structure and composition of their eggshell (chorion) constituent proteins.

2. Materials and methods

2.1. Sample preparation

All the eggs of *P. ricini* and *A. merione* examined in this study were obtained from cultures set up from 2nd and 3rd instar larvae trapped from castor plants at the vicinity of the Zoology Department, Allahabad University, India, and reared in the laboratory on castor leaves in troughs placed in an incubator at 28 ± 1 °C. The eggs were allowed to pupate and emerge. Freshly emerged adults were shifted to glass chimneys whose top was covered with thin cotton cloth impregnated with a 5% sucrose solution for feeding. Each chimney contained a single pair of insects and fresh castor leaves with stem for egg laying. After copulation, the females laid eggs in clusters on leaf lamina, initially by scrapping epidermal layers

* Corresponding author. Tel.: +30 210 7274931; fax: +30 210 7274254.
E-mail address: shamodr@biol.uoa.gr (S.J. Hamodrakas).
[1] These authors contributed equally to this work.

0141-8130/$ – see front matter © 2011 Elsevier B.V. All rights reserved.
doi:10.1016/j.ijbiomac.2011.05.006

and later by cutting the blades. Eggs were easily detached from the leaves with the help of a brush or a needle, fixed in Karnovsky's fixative [4] overnight at 4 °C for electron microscopy measurements and then shifted in a 0.1 M phosphate buffer kept at 4 °C.

For IR and Raman spectroscopic measurements, eggs were cut in half with fine needles and forceps and washed thoroughly several times with distilled water and sonicated to remove the oocyte and/or other remnants. The remaining, 'cleaned' eggshells (chorions) were then thoroughly dried in air.

2.2. Scanning electron microscopy

The eggs kept in 0.1 M phosphate buffer were transferred to alcohol and dehydrated in a graded alcohol series up to absolute alcohol and dried in a critical point drier apparatus (Polaron E 3000) at 20 °C using liquid CO_2 as a transitional fluid. Further, the eggs were mounted on copper stubs, coated with 35 nm gold in a sputter coater (Balzers SCD 020 Sputter Device) and viewed in a LEO 435 VP [UK] scanning electron microscope, operating at 15 kV.

2.3. Transmission electron microscopy

The eggs from 0.1 M phosphate buffer were transferred and dehydrated in a graded acetone series, infiltrated and embedded in araldite CY 212. Thin sections were cut by using glass knives in an ultramicrotome and mounted on 300 mesh copper grids. The sections were then stained by uranyl acetate (1%) and lead acetate (1%) and viewed under a Morgagni 268D transmission electron microscope (Fei Company, The Netherlands), operating at 80 kV. Digital images were acquired using a CCD camera (Megaview III, Fei Company, The Netherlands) and the software supplied with the microscope (Soft Imaging System, Munster, Germany).

2.4. Micro-Raman

Micro-Raman spectra were recorded on a dispersive confocal Raman microscope (Renishaw InVia Reflex, 1200 l/mm). Data were collected through a 50× lens using the 785 nm diode laser line for excitation. Several spectra were collected per sample and averaged. The total acquisition time was of the order of 1 h per sample.

2.5. Attenuated total reflectance infrared (ATR FT-IR) spectroscopy

Infrared spectra were recorded on a Fourier transform instrument (Equinox 55, Bruker Optics) equipped with a single-reflection diamond Attenuated Total Reflectance (ATR) accessory (DuraSamplIR II by SensIR). Both the spectrometer and the ATR accessory were purged by dry N_2 to reduce the effect of H_2O vapors on the spectra. Clusters of chorions were held in contact with the diamond element by means of a suitable press. With a penetration depth of the order of a few μm, ATR provides spectra free of optical saturation effects. Several spectra were measured, each representing the average of 100 scans at a resolution of 4 cm^{-1}. The measurement of each sample was bracketed between two background measurements to allow for the complete compensation of H_2O vapor. Average spectra are shown in the ATR absorption formalism, i.e., after correction for the wavelength-dependence of the penetration depth ($d_p \propto \lambda$).

2.6. Post-run computations of the spectra

In order to enhance the resolution of sharp features overlapping with broad bands, ATR FT-IR absorption band maxima were determined from the minima in the second derivative of the corresponding spectra. Derivatives were computed analytically by the Savitsky–Golay algorithm [5] using routines of the OPUS software (Bruker Optics) and included a 13-point smoothing. Given the zero-filling factor employed for the Fourier transform of the data, this smoothing range corresponds to ±12 cm^{-1}. Smoothing over narrower ranges resulted to a deterioration of the *S*/*N* ratio and did not increase the number of minima that could be determined with confidence.

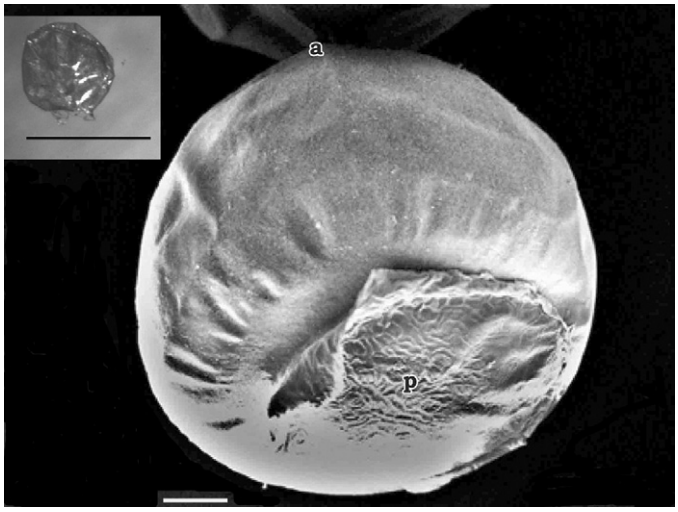

Fig. 1. Scanning electron micrograph of a laid egg of *Pericallia ricini*. The eggshell surface structure showing the anterior pole (a) and the posterior pole (p) is seen. Bar is 100 μm. Inset, shows a photograph taken under a dissecting microscope (stereo-microscope) of a 'cleaned' eggshell of *P. ricini*, used for IR and Raman measurements (see Section 2). Bar is 1 mm.

3. Results

3.1. Eggshell (chorion) morphology

The follicular cells surrounding the oocyte synthesize and secrete the proteins forming the eggshell (chorion) ([6] and Refs. therein). Fig. 1 is a scanning electron micrograph of an egg of *P. ricini*. The eggs have a spherical shape with a diameter ca. 720 μm. Fig. 1, inset, shows a photograph taken under a dissecting microscope (stereo-microscope) of a 'cleaned' eggshell of *P. ricini*, used for IR and Raman measurements (see Section 2). Fig. 2 shows a transmission electron micrograph taken from a thin, transverse (perpendicular to the surface of chorion) section through the chorion of *P. ricini*. The lamellar ultrastructure of chorion suggests a helicoidal architecture [3,6–8]. A similar lamellar ultrastructure is seen for the chorions of *A. merione* (data not shown).

Fig. 3 is a scanning electron micrograph of a laid egg of *A. merione*. The eggs seem to have a spherical shape, ca. 600 μm in diameter. The anterior pole of chorion contains the micropyle (M, white arrow) through which sperm entry occurs [9]. Respiratory appendages or respiratory filaments [9] (RF, white arrow), ca. 200–300 μm in length, protrude away from the surface of chorion, reminiscent of the spines (quills) of a porcupine or the spines of a sea urchin. The respiratory functions are facilitated by these long appendages arising from egg chorion as extrachorionic tubular projections [9]. Gravid females lay eggs in substrates and these respiratory appendages or filaments extend above the substrate surface thereby facilitating oxygen supply to the embryo and at the same time expulsion of carbon dioxide. The large numbers of appendages are there to meet the high oxygen requirements of the developing embryo/oocyte and to provide simultaneously protection from predators. Fig. 2, inset, shows a photograph taken under

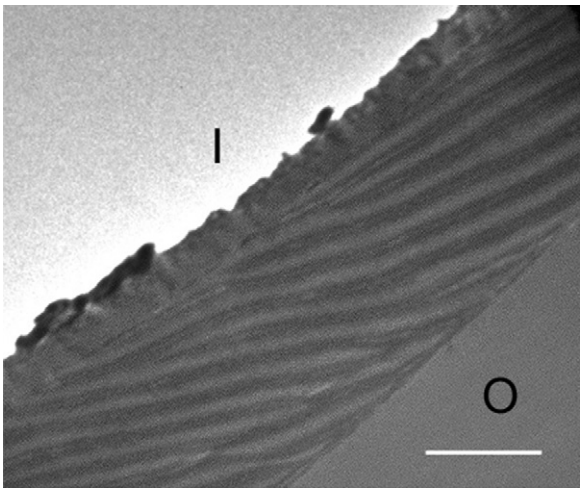

Fig. 2. Transmission electron micrograph of a thin transverse section cut through a *Pericallia ricini* eggshell (chorion). The lamellar structure of chorion is clearly seen, implying a helicoidal architecture for chorion (see text). I, is the inner (closest to the oocyte) part of chorion, O, is the outer surface of chorion. Bar is 1 μm.

a dissecting microscope (stereo-microscope) of a 'cleaned' eggshell of *A. merione*, used for IR and Raman measurements.

3.2. Vibrational spectra

The micro-Raman and ATR FT-IR spectra obtained from intact *P. ricini* and *A. merione* chorions are shown in Figs. 4a,b and 5a,b, respectively.

Inspection of these figures reveals that the vibrations of chorion proteins exhibit different activity in the Raman and IR spectra, as expected from the different selection rules applicable for the two techniques. This fact results to significant differences in the apparent maxima and convoluted bandshapes. The band maxima of the main spectral features are compiled in Table 1, together with their suggested assignments.

A rather striking observation, which is derived from direct comparison of the vibrational spectra as well as from the peak maxima compiled in Table 1, is that the spectra are very similar from the two species, despite the differences in morphology seen from the scanning transmission micrographs of the two eggshells. This is a strong indication for the existence of extensive similarities in the amino acid sequences of the proteins of both species and their relative proportions in both eggshells. Furthermore, it suggests similar secondary and, most probably, tertiary structures for these proteins.

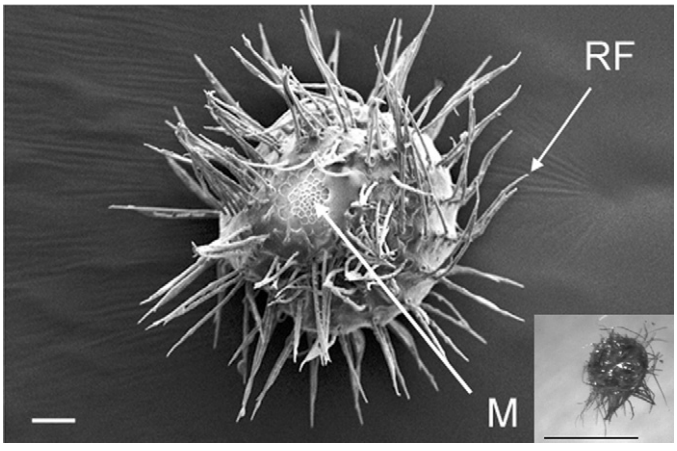

Fig. 3. Scanning electron micrograph showing the surface of a laid egg of *Ariadne merione*. The arrows point to the micropyle and the respiratory filaments of the chorion (M and RF, respectively). Bar is 100 μm. Inset, shows a photograph taken under a dissecting microscope (stereo-microscope) of a 'cleaned' eggshell of *A. merione*, used for IR and Raman measurements (see Section 2). Bar is 1 mm.

Table 1
Main micro Raman (1800–450 cm^{-1}) and ATR FT-IR (1800–700 cm^{-1}) band maxima of *Pericallia ricini* and *Ariadne merione* chorion spectra (outer surface). In the latter case, the band maxima were determined from the 2nd derivative spectra. Very strong bands are shown in bold. Tentative assignments are included. For details see text.

Micro Raman		ATR FT-IR		Assignment
Pericallia ricini	*Ariadne merione*	*Pericallia ricini*	*Ariadne merione*	
		1736	1736	–COOH
				Amide I
		1692	1692	Antparallel β-sheet
1675	**1673**			β-sheet
		1658	1658	β-turns? α-helix?
		1622	**1624**	β-sheet
1618	1618			Tyr (Phe, Trp?)
				Amide II
1557	1556	1543	1540	β-sheet
		1514	**1514**	Tyr
1454	**1453**	**1446**	**1448**	CH_2 deformation
		1406	1409	CH_3 deformation
		1385	1385	
		1370	1370	
				Amide III
1346	1342	1338	1338	Trp? β-turns?
1313	1316	1311	1310	β-turns? α-helix?
1275	1276	1270	1270	β-turns? random coil?
1242	**1243**	**1234**	**1234**	β-sheet
1209	1209			Tyr, Phe
1179	1175	1168	1168	Tyr
1126	1124	1125	1125	C–O stretching
			1104	
1091	1088	1078	1078	
1032	1032			Phe
1005	**1004**			Phe
932	920			
881	894			Trp
855	**852**			Tyr
831	**828**			Tyr
761	758			Trp
644	643			Tyr, Phe
622	621			Phe
514	515			S–S

No significant bands below 500 cm^{-1} were observed in the Raman spectra. Similarly, below ca. 1000 cm^{-1}, the ATR FT-IR spectra exhibit only a rather featureless broad envelope. Several bands are clearly assignable to side chain vibrations of amino acid residues, especially to the aromatic ring-containing Tyr, Trp and Phe. In the following paragraphs peak positions are given for *P. ricini*. Those corresponding to *A. merione*, if different by more than 1 cm^{-1} are given in parentheses.

Thus, Raman bands at 1032, 1005, and 622 cm^{-1} are ascribable to Phe, whereas those at 644, 831 (828), 855 (852), 1209 and 1618 (1616) cm^{-1} are most likely due to Tyr, with possible contributions from Phe at 644, 1209 and 1609 cm^{-1}, or Trp [10–12]. The intensity ratio of the tyrosine doublet at ca. 855 (852) and 830 (828) cm^{-1}, $R = I_{855}/I_{830}$, is sensitive to the nature of hydrogen bonding or to the state of the dissociation of the phenolic hydroxyl group and has been used to identify "buried" and "exposed" Tyr moieties ([13] and Refs. therein). In our case this ratio is ca. 1.1–1.2, in both Raman spectra, and indicates that tyrosines are exposed and their phenolic hydroxyl groups act as very weak hydrogen bond donors or as acceptors to acidic protons. Tyr may also contribute to infrared absorption and Raman scattering at ca. 1270 and 1500–1515 cm^{-1} [14,15]. Raman bands at 761 (758) and 881 (894) cm^{-1} are ascrib-

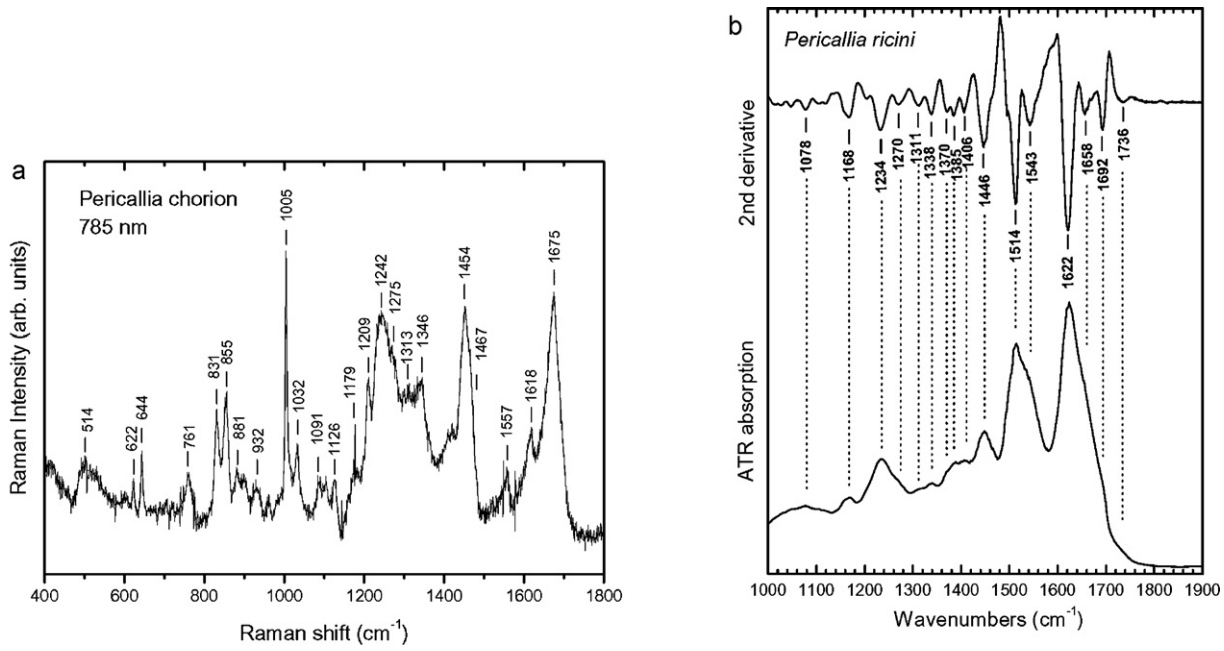

Fig. 4. (A) Raman and (B) ATR IR spectra of *Pericallia ricini*. In (B), the second derivative of the spectrum (top part) is included.

able to Trp [10–12]. The absence of a band at 1361 cm^{-1} suggests that the Trp units are, presumably, not "exposed" [11,16].

Raman bands in the 500–550 cm^{-1} region are typically associated with the S–S stretching mode of the C–C–S–S–C–C structural unit of disulphide bonds [10–12]. According to Edwards et al. [17] the bands at 506 cm^{-1} in the FT-Raman spectra of keratins may be assigned to S–S bridges in *g*–*g*–*g* conformation. The rather strong bands at ca. 514 cm^{-1} in the Raman spectra of *P. ricini* and *A. merione* chorions are presumably of the same origin.

Following this description of the vibrational signatures of the side groups, we focus at the "amide" band envelopes, which are well known secondary structural indicators in proteins and polypeptides. Several works review the relevant assignments of the Raman [10–13,18,19] and IR [14,15,20–25] spectra in the Amide I, II and III regions. These assignments are summarized for convenience in Table 2.

In the Amide I region (1600–1700 cm^{-1}) the Raman spectra of the *P. ricini* and *A. merione* chorions exhibit well defined maxima at 1675 and 1673 cm^{-1}, respectively (Figs. 4a and 5a and Tables 1 and 2), whereas the ATR spectra are peaking at 1622 and 1624 cm^{-1}, respectively (Figs. 4b and 5b and Tables 1 and 2). Both positions are typical of β-sheet structure. The 2nd derivative ATR spectra of both chorions reveal also the presence of a sharp Amide I component at 1692 cm^{-1}, which can also be discerned as a shoulder in the absorption spectra. There is some disagreement in the literature about the origin of bands in the 1670–1695 cm^{-1}

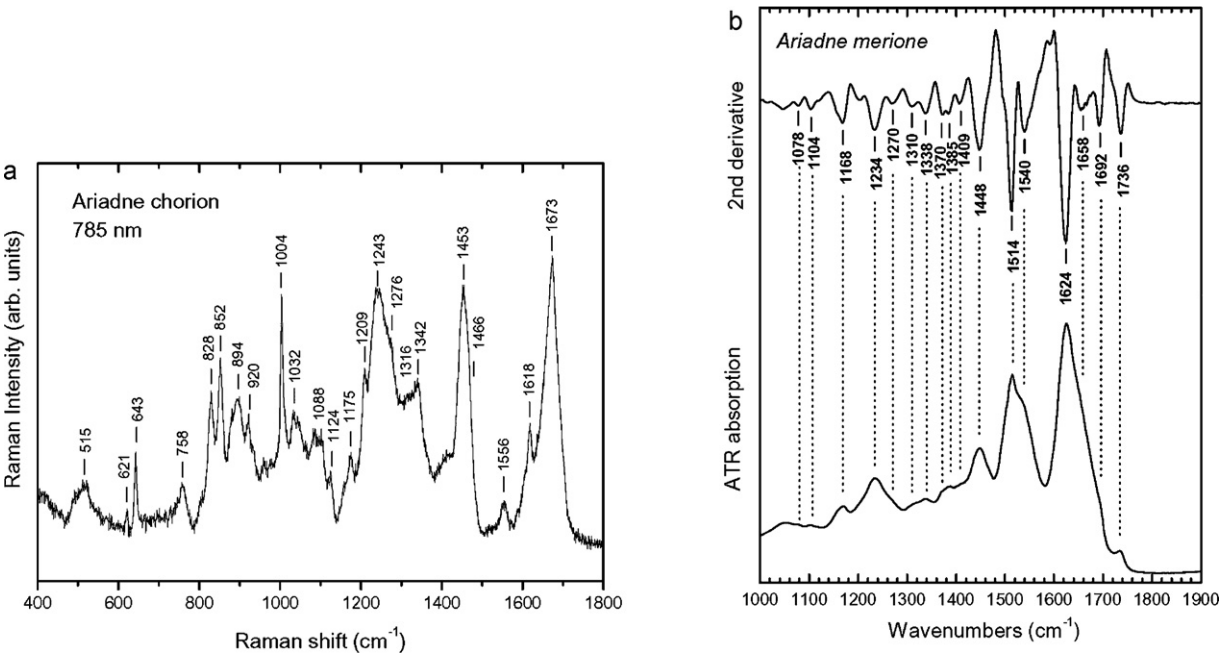

Fig. 5. (A) Raman and (B) ATR IR spectra of *Ariadne merione*. In (B), the second derivative of the spectrum (top part) is included.

Table 2
Amides I, II and III infrared and Raman wavenumber ranges and their dependence on secondary structure. Band maxima obtained from *P. ricini* and *A. merione* (**in parentheses**) chorions are included for comparison. Wavenumbers are in cm^{-1}.

	α-Helix		β-Sheet		β-Turns		Random/unordered		*P. ricini* (*A. merione*)	
	Infrared	Raman	Infrared	Raman	Infrared	Raman	Infrared	Raman	Infrared	Raman
Amide I	1644–1649[a] or 1653–1660[b]	1645–1663[d,e]	1691–1699[a] or 1610–1640[a,b,f]	1665–1680[d,e]	1662–1695[d]	1665,1690[d]	1650–1654[a] or 1640–1650[b]	1649–1665[e] (broad)	1692 (1692) 1658 (1658) 1622(1624)	1675 (1673)
Amide II	1548–1553[a] or 1519–1521[a]	1545[d] 1516[d]	1563[a] or 1530–1535[a]	1560[d] 1535[d]		1560–1567[d] 1545–1555[d]	1546–1553[a]		1543 (1540)	1557 (1556)
Amide III	1280–1317[c]	1260–1295[d]	1230–1245[c]	1230–1243[d,e,g]		1290–1330[d]	1245–1270[c]	1243–1249[e]	1338 (1338) 1311 (1310) 1270 (1270) 1234 (1234)	1346 (1342) 1313 (1316) 1275 (1276) 1242 (1243)

[a] Venyaminov and Kalnin [14,15].
[b] Griebenow et al. [25].
[c] Singh et al. [20,28].
[d] Orfanidou et al. [3].
[e] Carey [13].
[f] 1610–1625 intermolecular; 1630–1640 intramolecular (Griebenow et al. [25]).
[g] Often appears split into 1233 and 1245 cm^{-1} components (Singh et al. [20]).

region ([23] and Refs. therein). In proteins containing antiparallel β-sheets, a high frequency β-sheet component that arises from transition dipole coupling is usually found at 50–70 cm^{-1} higher than the main β-sheet component ([24] and Refs. therein). Alternatively, bands in this region may be due to β-turns joining strands of β-sheets, and, consequently, part of the β-sheets themselves. Finally, the 2nd derivative ATR spectra of both chorions exhibit a weak (hence, broad) band at ca. 1660 cm^{-1} the apparent position of which is shifted towards higher wavenumbers by the neighbouring dominant 1622/1624 cm^{-1} band. As the Amide I spectra are dominated by strong features attributed to β-sheets, it is difficult to distinguish whether the 1660 cm^{-1} IR feature is due to β-turns or α-helices. Finally, the IR spectra of the *A. merione* (and to a lesser extend *P. ricini*) chorions exhibit a band at 1736 cm^{-1}, which is tentatively attributed to protonated calboxylate groups of Glu or Asp side chains (C=O stretching). Altogether, the Amide I bands both from Raman and IR spectra of intact *P. ricini* and *A. merione* chorions, strongly suggest that the most abundant secondary structure of chorion proteins is the β-sheet. The β-sheets are most probably antiparallel.

The Amide II vibrations are located at ca. 1557 cm^{-1} in the Raman spectra and 1543 (1540) cm^{-1} in the infrared spectra. The strong 1514 cm^{-1} infrared band is tentatively assigned to Tyr ring vibrations. Although the Amide II bands are considered of reduced diagnostic value as secondary structural proxies, the IR bands are consistent with abundant β-sheet in chorion proteins, in both species [23,25]. While we assign the strong 1514 cm^{-1} infrared band to Tyr ring vibrations, it is interesting to note that poly-Gly I, an antiparallel β-pleated sheet structure, exhibits a strong amide II IR band at 1517 cm^{-1} [26].

The Amide III infrared range (1230–1320 cm^{-1}) is relatively free from side-group vibrations and, thus, highly diagnostic of secondary structure. Typically, the Amide III range can be split in three regions 1320–1280 cm^{-1}, 1270–1245 cm^{-1} and 1245–1225 cm^{-1}, indicative of α-helices, random structures and β-sheet, respectively [27,28]. The strongest Amide III infrared bands of both *P. ricini* and *A. merione* chorions are observed at 1234 cm^{-1}, while additional bands are seen at 1270 and 1311 cm^{-1}. The corresponding Raman spectra exhibit their strongest maximum at 1242 cm^{-1} with a shoulder at 1275 cm^{-1}, as well as a difficult to resolve feature at ca. 1315 cm^{-1}. The 1234 cm^{-1} infrared band and the 1242 cm^{-1} Raman band are clearly assignable to β-sheets. Infrared and Raman bands in the 1310–1315 cm^{-1} range may be indicative of α-helices. Vibrational activity at ca. 1270 cm^{-1} in both the infrared and Raman spectra is most probably associated with the presence of unordered (random coil) structure or β-turns. Both the infrared and Raman spectra exhibit a strong feature at ca. 1340 cm^{-1}. This band falls outside the normally accepted range for Amide III vibrations, although assignments of similar features to β-turns have been attempted [18]. Alternatively, we suggest that this feature could be attributed to a side-chain N–H vibration, which is sensitive to secondary structure.

4. Discussion

This study reveals that the chorions of the Lepidoptera species, *P. ricini* and *A. merione* adopt a helicoidal architecture, which is common to several other Lepidoptera species, such as the wild type silkmoth *Antheraea polyphemus*, the domesticated silkmoth *Bombyx mori* ([6] and Refs. therein), the tobacco hornworm *Manduca sexta* and the pest *Sesamia nonagrioides* [3]. The occurrence of the helicoidal architecture is widespread not only to Lepidoptera but also in the chorion (also referred to as *Zona pellucida*) of fishes [7,29] and also in helicoids which are not simply proteinaceous, but are bi-composites of polysaccharide (chitin) and protein, like the cuti-

cle of arthropods [8,30,31] or are composed only of polysaccharides (cellulose [32–34]).

On the basis of the vibrational data it is evident that the *P. ricini* and *A. merione* chorions consist of proteins which adopt primarily an antiparallel β-pleated sheet conformation, with a contribution from β-turns and, maybe, a minor participation of α-helical and random segments. This structural picture is similar to that deduced for all Lepidoptera chorions accounted to date [3,6]. Twenty-seven years ago, we have proposed that the common molecular denominator of the helicoidal architecture is the β-sheet [35]. The present findings add to the ample experimental support for this early proposal, which extends to systems where the proteins are involved in combination with polysaccharides [34].

These common morphological and architectural features of the Lepidoptera chorions allow them to play the role of the first known, functional, protective amyloids ([36,37] and Refs. therein).

Still, the formation of these chorions from their constituent proteins, by a self-assembly process, on the surface of the oocyte, away from the follicular cells that synthesize them, is far from being understood. To envisage how these β-sheets interact to form a three-dimensional helicoidal architecture, requires also, at least, a detailed knowledge of the corresponding aminoacid sequences of the chorion proteins from both species. Unfortunately, the sequences of these proteins are not available to date.

Acknowledgments

We thank the University of Allahabad, India for financial support and the Division of Electron Microscopy, All India Institute of Medical Sciences (AIIMS), New Delhi, India, for providing facilities and technical assistance. We also thank the University of Athens and National Hellenic Research Foundation for financial support. We should also like to thank the reviewers of this manuscript for their useful and constructive criticism.

References

[1] K. Asafali, R.S. Perumal, T.R. Subramanian, Madras Agric. J. 59 (1972) 566–570.
[2] J.B. Atluri, B. Samantha, M. Bhupathi Rayalu, D. Sandhya Deepika, C. Subba Reddi, J. Res. Lepi. 42 (2010) 13–20.
[3] C.C. Orfanidou, S.J. Hamodrakas, G.D. Chryssikos, E.I. Kamitsos, S.E. Wellman, S.T. Case, Int. J. Biol. Macromol. 17 (1995) 93–98.
[4] M. Karnovsky, J. Cell Biol. 27 (1965) 137A–138A.
[5] A. Savitsky, M.J.E. Golay, Anal. Chem. 36 (1964) 1627–1639.
[6] S.J. Hamodrakas, Results Probl. Cell Differ. 19 (1992) 115–186.
[7] P. Papadopoulou, V.K. Galanopoulos, S.J. Hamodrakas, J. Struct. Biol. 116 (1996) 399–412.
[8] A.C. Neville, Phys. Bull. 37 (1986) 74–76.
[9] L.H. Margaritis, F.C. Kafatos, W.H. Petri, J. Cell Sci. 43 (1980) 1–35.
[10] B.G. Frushour, J.L. Koenig, Biopolymers 14 (1975) 2115–2135.
[11] N.T. Yu, CRC Crit. Rev. Biochem. 4 (1977) 229–280.
[12] T.G. Spiro, B.P. Gaber, Annu. Rev. Biochem. 46 (1977) 553–572.
[13] P.R. Carey, Biochemical Applications of Raman and Resonance Raman Spectroscopies, Academic Press, New York, 1982.
[14] S. Venyaminov, N.N. Kalnin, Biopolymers 30 (1990) 1243–1257.
[15] S. Venyaminov, N.N. Kalnin, Biopolymers 30 (1990) 1259–1271.
[16] M.C. Chen, R.C. Lord, R. Mendelsohn, Biochim. Biophys. Acta 328 (1973) 252–260.
[17] H.G.M. Edwards, M.J. Falk, M.G. Sibley, J. Alvarez-Benedi, F. Rull, Spectrochim. Acta Part A – Mol. Biomol. Spectrosc. 54 (1998) 903–920.
[18] J. Bandekar, S. Krimm, Proc. Natl. Acad. Sci. U.S.A. 76 (1979) 774–777.
[19] P.R. Carey, V.R. Salares, Raman and Resonance Raman Studies of Biological Systems, Academic Press, Heyden/London, 1980.
[20] B.R. Singh, M.P. Fuller, G. Schiavo, Biophys. Chem. 36 (1990) 155–166.
[21] E. Goormaghtigh, V. Cabiaux, J.M. Ruysschaert, Eur. J. Biochem. 193 (1990) 409–420.
[22] W.K. Surewicz, H.H. Mantsch, D. Chapman, Biochemistry 32 (1993) 389–394.
[23] P.I. Haris, D. Chapman, Biopolymers 37 (1995) 251–263.
[24] M. Jackson, H.H. Mantsch, Crit. Rev. Biochem. Mol. Biol. 30 (1995) 95–120.
[25] K. Griebenow, A.M. Santos, K.G. Carrasquillo, Internet J. Vib. Spectrosc. 3 (1999) 1–34.
[26] S. Krimm, J. Bandekar, Adv. Protein Chem. 38 (1986) 181–364.
[27] F.N. Fu, D.B. Deoliveira, W.R. Trumble, H.K. Sarkar, B.R. Singh, Appl. Spectrosc. 48 (1994) 1432–1441.
[28] B.R. Singh, M.P. Fuller, Appl. Spectrosc. 45 (1991) 1017–1021.
[29] J.P. Grierson, A.C. Neville, Tissue Cell 13 (1981) 819–830.
[30] A.C. Neville, Biology of the Arthropod Cuticle, Springer-Verlag, Berlin/Heidelberg/New York, 1975.
[31] A.C. Neville, Mol. Cryst. Liq. Cryst. 76 (1981) 279–286.
[32] Y. Bouligand, Tissue Cell 4 (1972) 189–217.
[33] Y. Bouligand, Abstracts of Papers of the American Chemical Society 174 (1977) 20–120.
[34] Y. Bouligand, Liquid Crystalline Order in Biological Materials, Academic Press, New York/San Francisco/London, 1978.
[35] S.J. Hamodrakas, International Journal of Biological Macromolecules 6 (1984) 51–53.
[36] V.A. Iconomidou, G. Vriend, S.J. Hamodrakas, FEBS Lett. 479 (2000) 141–145.
[37] V.A. Iconomidou, S.J. Hamodrakas, Curr. Protein Pept. Sci. 9 (2008) 291–309.